Manufacturing of an airborne demonstrator of ALADIN, the direct detection Doppler wind lidar for ADM-Aeolus

Y. Durand [(a)], R. Meynart [(a)], M. Endemann[(a)], E. Chinal[(b)], D. Morançais [(b)], T. Schröder[(c)], O. Reitebuch [(c)]

[a] ESA-ESTEC, Earth Observation Programmes P.O. Box 229, 2200 AG Noordwijk, the Netherlands

[b] EADS-Astrium SAS, 31 rue des cosmonautes, 31402 TOULOUSE Cedex 4, France

[(c)] DLR Institut für Physik der Atmosphäre, Münchener Str. 20, 82234 Wessling, Germany

ABSTRACT

Due for launch in 2008, the Atmospheric Dynamics Mission (ADM-Aeolus) has been selected as ESA's second Earth Explorer Core Missions within its Living Planet Programme. Its payload aims at providing measurements of atmospheric wind profiles with global coverage. The key element of ADM-Aeolus is the Atmospheric LAser Doppler Lidar INstrument (ALADIN), a Direct Detection Doppler Lidar in the ultra-violet spectral region operating on aerosol and molecular backscatter signals in parallel. The ALADIN instrument belongs to a completely new class of active optical earth-observation payloads with limited power requirements and high reliability over a three-year lifetime. It will be the first European Lidar in space. Technological challenges have been addressed in an early stage by a pre-development programme that consisted of designing, manufacturing and testing a functional representative model of the receiver of ALADIN (the Pre-Development Model, PDM), and a breadboard of the transmitter. The pre-development programme has been successfully completed and both receivers and transmitter are being refurbished in an airborne configuration.
The ALADIN airborne instrument demonstrator (A2D) will be used for ground and airborne campaigns prior to the launch of the satellite. This paper presents the main characteristics of the airborne instrument and the goals of the campaigns.

Keywords: ALADIN, ADM-Aeolus, wind lidar, airborne demonstrator

1. INTRODUCTION

The primary aim of the ADM-Aeolus mission is to provide global observation of vertical wind profiles. After several decades of earth observation from space, direct measurements of the global wind field remain limited however crucial for understanding the dynamic of the atmosphere and further improving the numerical weather prediction systems as well as the climate modelling [(1)]. Spaceborne Doppler lidars offer the unique potential to accurately measure wind profiles in the troposphere and the lower stratosphere (0-27 km) both in clear air and partially cloudy atmosphere[(2,3)].

The concept of the Aeolus mission is explained in figure 1. A very high performance Doppler Wind Lidar, called ALADIN, will be accommodated on a satellite flying in a sun-synchronous dawn-dusk orbit at an altitude of 400 km and will provide near-global coverage [(4)]. The lidar is an active instrument that fires pulses of laser light toward the atmosphere along a line of sight (LOS) with a 35º slant angle with respect to Nadir direction, oriented across track. In the return signal, backscattered light from the air molecules at high altitudes and from aerosols at lower altitudes is collected and its Doppler frequency shift is measured. The Doppler shifts depend on the velocity in LOS direction of the scattering particles, providing the determination of the projection of the horizontal wind onto the LOS for every altitude. In order to increase the accuracy, 700 wind profiles are averaged during 7 seconds, which corresponds to a 50 km line on ground. The measurement is repeated every 28 seconds, which corresponds to every 200 km along the orbit. The vertical resolution is determined by techniques of time gating the return signal. At low altitudes, a resolution of 500 m is required, extending to 1 km in the troposphere and to 2 km above a 16 km altitude.
A direct detection UV concept at 355 nm provides a scattering ratio (ratio between the total scattering and molecular scattering) close to unity. It was selected as the best compromise in terms of performance, technical risk and eye safety on ground. The laser source is based on a single-mode, 150 mJ, 100 Hz pulse/repetition frequency, diode-pumped and frequency-tripled Nd-YAG laser. The receiver consists of two interferometers one for the Mie spectrum, one for the

Rayleigh spectrum, providing an optimal performance over the whole altitude range. The molecular channel (Mie) is based on a Fizeau interferometer whereas the aerosol channel (Rayleigh) uses the dual filter or double-edge technique with a sequential Fabry-Perot interferometer.

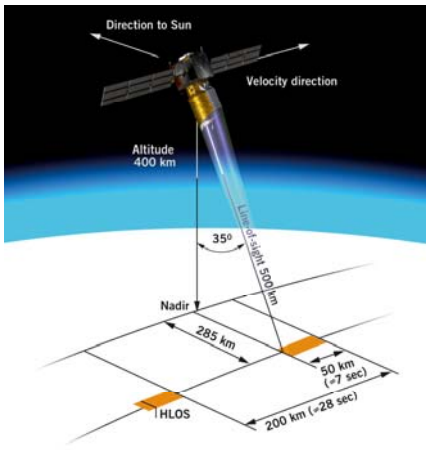

Figure 1: ADM-Aeolus measurement geometry. The lidar emits a laser pulse toward the atmosphere, then collects, samples and retrieves the frequency of the backscattered signal.

The instrument concept of ALADIN combines new techniques, like a novel combination of the molecular and aerosol receiver, the use of an accumulation CCD. Moreover the transmitter programme is demanding in term of lifetime, energy per pulse and frequency stability. All these technical challenges have been addressed in a risk reduction programme that encompasses [5]:

a) A laser transmitter programme, including

Two parallel developments of laser breadboards to demonstrate the feasibility of a single frequency tuneable diode-pumped Nd:YAG laser providing 150 mJ per pulse at 355 nm, operating in burst mode with 100 Hz PRF during 7 seconds, every 28 seconds.

Testing of commercial continuous laser diodes and commercial pulsed laser diode arrays used respectively for pumping the seeder, and the oscillator and the amplifier stages of the laser transmitter. The laser diodes are tested in various stress conditions allowing accelerated life testing to determine potential failure mechanisms. Tests are made in vacuum and atmospheric conditions.

Separate studies of specific technology improvements (e.g. optimisation of frequency tripling efficiency, solid-state phase-conjugation mirrors).

b) A lidar receiver programme, consisting of a full Pre-Development Model (PDM) of the key receiving parts of the instrument, in a system and sub-system configuration as representative as possible of the design, materials and building techniques of the flight model.

c) An airborne instrument demonstrator combining the refurbished PDM and laser transmitter for ground and airborne campaigns. The main objectives of the campaigns are to validate the predicted instrument performance and to obtain a dataset of atmospheric measurements which will be used before launch to test and validate the algorithms and quality control scheme and to allow the final selection of instrument parameters for optimised in-orbit measurement performance. The ALADIN Airborne Demonstrator (A2D) is currently under development at EADS-Astrium, France, EADS-Astrium, Germany and DLR, Germany. The receiver consists of the refurbished PDM developed by EADS-Astrium, France and the laser transmitter is based on the laser breadboard previously developed by EADS-Astrium,

Germany. Specific aircraft hardware and ground support equipment are manufactured by DLR, Germany who will run the campaigns onboard a Falcon aircraft.

The paper presents first the architecture of the ALADIN Airborne Instrument Demonstrator (A2D) then reports on the results obtained during the preliminary tests. At last the objectives of both ground and airborne campaigns are detailed.

2. A2D LASER TRANSMITTER

2.1 Laser Design

The laser source is based on the previously developed breadboard laser from EADS-Astrium, Germany. It relies on a diode-pumped tripled Nd:YAG laser and consists of an optical head, a control electronics and a thermal control system. **Table 1** summarises the main optical specifications of the airborne transmitter compared to the end of life specifications of the satellite transmitter. Unlike the spaceborne transmitter, the laser emits pulses at 50 Hz continuously. The primary goal of the burst mode being to save energy on board the satellite, the burst mode was discarded for the airborne system simplifying the laser design. The energy per pulse has been optimised to take into account the lower flying altitude and the lower telescope diameter while maintaining the expected levels of signal on the receiver. Polarisation and divergence differ only at transmitter level, but the routing optics functions being different for the airborne and the satellite they have comparable values at the output of the telescope: circular polarisation in both cases, and 10 µrad divergence for the satellite.

Table 1: Transmitter optical requirements

Parameters	Airborne	Satellite
Energy per pulse	70 mJ	150 mJ
Pulse repetition rate	50 Hz	100 Hz in burst mode
Polarisation	Circular, purity > 100:1	Linear, better than 100:1
Pulse duration	< 100 ns and > 15ns FWHM	< 100 ns and > 15 ns FWHM
Pulse linewidth	< 50 MHz	< 50 MHz FWHM
Spectral purity	99 % within 125 MHz	99% of the pulse energy within 90 MHz
Frequency stability	4 MHz rms over 14 s	4 MHz rms over 7s
Tunability	± 5 GHz	± 12.5 GHz
Divergence	< 55 µrad and > 50 µrad	< 400 µrad

The optical design consists of three main parts: a reference laser, a power laser and a frequency conversion stage. The reference laser is used as injection seeder for a low power oscillator in order to achieve single frequency operation and tuneability. The amplification is achieved in two stages in order to reach the required energy. Harmonic sections convert the IR beam to a green then UV beam at 355 nm. The optical layout of the A2D laser is shown in Figure 2. It meets the given envelope requirements of 344 mm width, 780 mm long and 352 mm high.

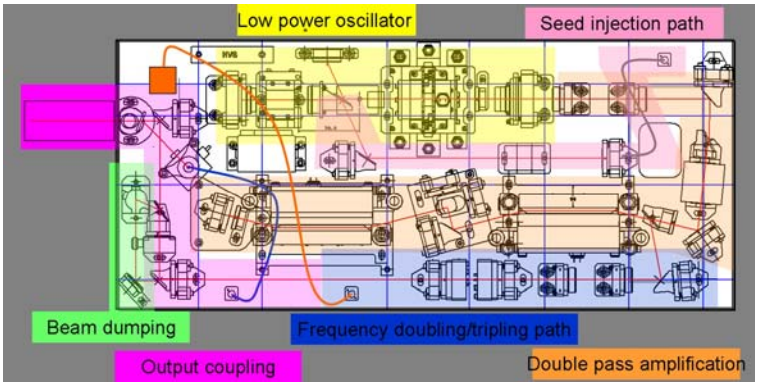

Figure 2: Transmitter optical layout with blocks coloured by function.

The design of the low power oscillator cavity is linear, and is mainly composed of the pump unit and two resonator mirrors to build a positive branch unstable resonator. The pump unit is composed of a Nd:YAG rod transversally pumped by 3 standard stacks in a 3-fold radial symmetric configuration. Each stack provides a peak power of 500 W for 175 µs pulse duration at 100 Hz. The pumping structure holds firmly the rod and the diode stacks while allowing an effective cooling. The output coupler is a Gaussian mirror, which ensures well output beam parameters. The length of the resonator is about 30 cm. To prevent the effect of spatial hole burning in the laser crystal, two Quarter-wave plates are placed in front of and after the diode pump structure to have a circular polarization within the rod (twisted mode cavity). For the generation of actively controlled laser pulses a polarizer, a quarter wave-plate and a pockels cell as Q-switch are inserted. The oscillator is injection seeded to reduce the linewidth of the output pulse and obtain the required tuneability.

The Reference Laser Head (RLH) is a low power (cw) frequency tunable IR laser system with high frequency stability (Figure 3). The RLH consists of two identical laser systems (reference laser and seed laser) and a frequency stabilization scheme. The reference laser -being the frequency reference- operates as a quasi fixed-frequency laser, while the seed laser needs to be a continuously frequency tuneable laser. Reference and seed laser are both Nd:YAG laser crystals based on a non planar ring geometry, which allows to combine high frequency stability and tunability in the same device. The laser crystal is optically pumped by laser diodes at about 808 nm and it emits laser radiation at 1064 nm. The laser output radiation passes a faraday isolator to avoid interfering backreflections into the laser crystal and it is finally coupled into a polarisation maintaining single-mode fiber connected with the optical interface to the oscillator. Coupling into the oscillator cavity occurs through a polarizer.

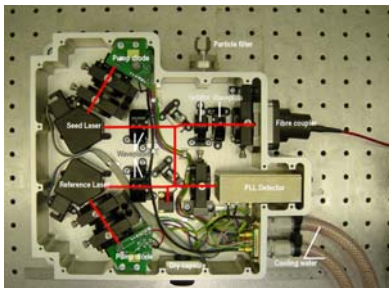

Figure 3: Reference laser head

While the cw seed laser frequency of the RLH is injected into the resonator cavity the closed Q-switch prevents the lasing during the pumping time of about 175 µsec. At the end of the pump pulse the Q-switch will be opened and the seeded laser light will be amplified at the same frequency - provided the actual resonator mode fits “exactly” with the seeded frequency. Otherwise the seed frequency would drift to the next resonant spectral line.
The cavity length is controlled by the method of minimization of the pulse build-up time. This principle is based on the fact, that the pulse generation time in the resonator is shorter if the pulse starts from the photons of the seed laser than if the pulse starts from the spontaneous emitted photons. For this operation principle it is necessary to jitter the oscillator cavity length symmetric around the optimum configuration, which leads to an output pulse frequency at two alternating values with a distance of a few MHz (IR). By use of every second pulse of the oscillator for the high power pulse generation it is possible to optimize the frequency stability of the UV output to a level inside the requirement of < 4MHz over 14s.

A slab geometry has been selected as baseline for the two amplifier stages. This geometry allows effective removal of the strong thermal load deposited in the slab by the pump laser light. The Nd:YAG slab dimensions have been determined through optical and thermo-optical simulations to ensure an effective extraction. When double passed, eleven internal reflections have been determined as an optimum fill factor at given beam diameter and slab dimensions. Each slab is side-pumped by 8 standard stacks (1000 W/stack for about 175 µs pulse duration at 50 Hz, synchronized on the oscillator). The pump unit holds the slab without stress and evacuate the consequent heat load

coming from the diodes and the slab. The cooling of the diodes and the slab is completely decoupled: the slab is glued on an aluminium structure cooled by one water pipe and the diodes are fixed to a copper mount cooled by two water pipes.

Between the two slabs, three mirrors allow to rotate the beam spatially by 90°. In this manner a spherical mirror can be used for the return pass. The rotation allows to use only spherical optics for thermal lens compensation. After double pass amplification the beam is quasi circular so that a spherical telescope is used before the harmonic section.

The harmonic crystals are LBO crystals. Their mounts are identical. The only difference is the crystal length. SHG crystal is 18 mm long while THG crystal is 16 mm. Section is 7 x 7 mm^2 for both crystals. The LBO is held between two aluminium parts where an Indium foil is placed between the crystal and the aluminium mount to optimize the thermal conductance. Four heaters allow to heat the mount symmetrical to a optimum operation temperature above the environmental level. A thermistor is attached to the mount for temperature regulation. A commercial regulator insures temperature setting.

All optical components are mounted on a baseplate made of Invar (Figure 4). The main reasons for the selection of this material are the specified large temperature changes in the non-operational mode from 3°C to 37°C and in the operational mode from 12 to 37 °C and the possible temperature gradients by external temperature distribution and internal "warm" spots (pump units). It guaranties optimized thermo-mechanical stability for a long time. The baseplate is custom designed and a milled part.

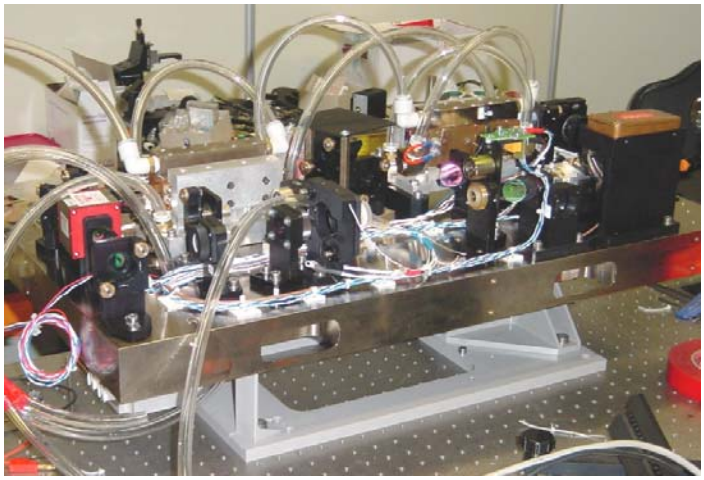

Figure 4: ALADIN airborne transmitter during integration

In order to cope with the environment of the aircraft, a cover closes the overall laser. The covers ensures protection against contamination (dust, liquids), accidental touch on optical elements (misalignment, scratches, damage), electro-magnetic disturbances in susceptibility as well as in emission, humidity, fast temperature changes, pressure differences and laser radiation. The cover is made of three layers: inner GFK housing, outer GFK housing, in between Airex R.82 foam and Aluminium foil.

The thermal design has to cope with ground operation and flight operation. All three pump units and the heat dump for the waste beams will be cooled by a closed water loop. The Falcon heat exchanger is part of the Falcon aircraft and can handle thermal loads up to 1kW. The cooling of the transmitter consists of two separated cooling circuits. The primary circuit flows through the laser head. Its inlet temperature is controlled by a custom made cooling unit in 19" rack. For ground operation an additional chiller is provided. The external chiller is connected to separate connectors with valves. It also permits to fill the closed water loop with the necessary water pressure.

2.2 Laser Test results

During the initial phase of manufacturing a first spectral characterisation of the oscillator has been performed in order to check the frequency stability that can be obtained with the pulse build up time technique. First the Low Power Oscillator (LPO) FSR was measured to 405 MHz by scanning the cavity length and measuring the pulse build up time per pulse. The build up time reduction was of the order of 20 ns. The frequency stability was measured by a time resolved beat measurement between the output of the LPO and the a fraction of the RLH signal, frequency shifted by 200 MHz. Seed power was optimised by measuring the spectral stability to a value of 25 mW. From the results displayed in Figure 5, it can be deduced that the cavity control principle is able to stabilise the pulse output frequency to an accuracy close to 1 MHz rms over 700 shots. LPO linewidth is below 15 MHz. Tunability with frequency steps from 10 MHz to 50 MHz was verified without change noticeable in the beat frequency.

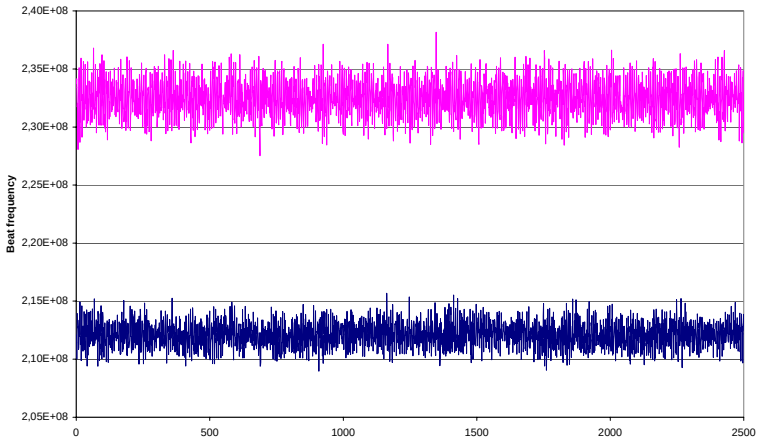

Figure 5: Measured beat frequency odd and even number of points, measured for every single shot by a heterodyne unit.

At last, performance of the LPO design against temperature changes was tested. For this measurement two 40W heating resistors were mounted at the baseplate close to the HR mirror of the LPO. With this setup a baseplate heating of 0.2K/min was measured in the middle of the resonator. This distance between heat source and temperature detector is the reason for the time delay between heating time and temperature change visible in Figure 6. Due to the strong cavity length change of the resonator (about 8µm/K) the cavity controller dynamic range for the piezo was not large enough to stay locked over this measurement. This can be seen at the frequency peaks during the measurement, where the cavity controller is loosing the lock. At the end of the measurement a second disturbing effect can be seen. The continuity between high jitter and low jitter is lost due a cavity control reset. Following these observations, an adaptation of the dynamic range has been performed.

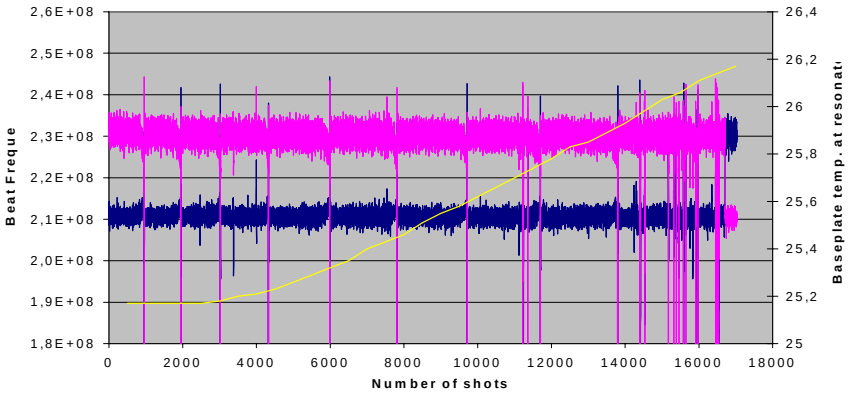

Figure 6: frequency measurement during baseplate heating. The yellow line provides the temperature in the middle of the resonator.

Environmental tests have been performed to verify the laser performance under all loads induced by environment during ground and flight operation (flight vibrations) and after all applied loads induced by the environment during non-operation intervals (landing, taxiing). Furthermore the laser airworthiness with respect to safety during flight has been controlled by dedicated EMC conductive and emission tests and a thorough review of the mechanical design.

Micro-vibration test with specified vibration spectra during flight have revealed non-compliances which translate by loosing the locking of the oscillator. As the damping properties of the frame on which the laser transmitter will be integrated are not fully characterized it has been deemed necessary to proceed to a test flight to check the behavior of the laser in its real flight environment.

At last the spectral stability of the RLH has been tested during temperature changes of the laser environment. The test was performed in a thermal chamber made of "Styrodur". The volume in the chamber was temperature controlled by an air conditioner allowing to blow temperature controlled air into it, simulating the temperature profile of the cabin air. During the test, RLH laser light was coupled out by fiber, frequency doubled into green light, frequency shifted by an AOM and mixed with an iodine stabilized laser. The beat frequency gave the frequency stability. From the measurements, the temperature sensitivity of the RLH to air temperature was measured down to 166 kHz/K and to water temperature as low as 13 MHz/K. The expected short-term stability of the RLH is then 200 kHz pp within 14 s of a measurement.

3. A2D RECEIVER

The receiver unit is based on the refurbished PDM. The PDM is a functional representative model of the receiver part of the ALADIN instrument, composed of engineering- model units going from the receiver/transmitter optics to the detection chain. Modifications of the PDM were necessary to comply with the airborne configuration.

Fig. 7 illustrates the mechanical and optical configuration of the A2D. The main critical sub-units (optical bench, Mie and Rayleigh spectrometers, detection front end unit, accumulation CCD) have been manufactured, characterized and integrated during the PDM programme. The units developed for the airborne instrument are the front optics, the routing optics and the telescope.

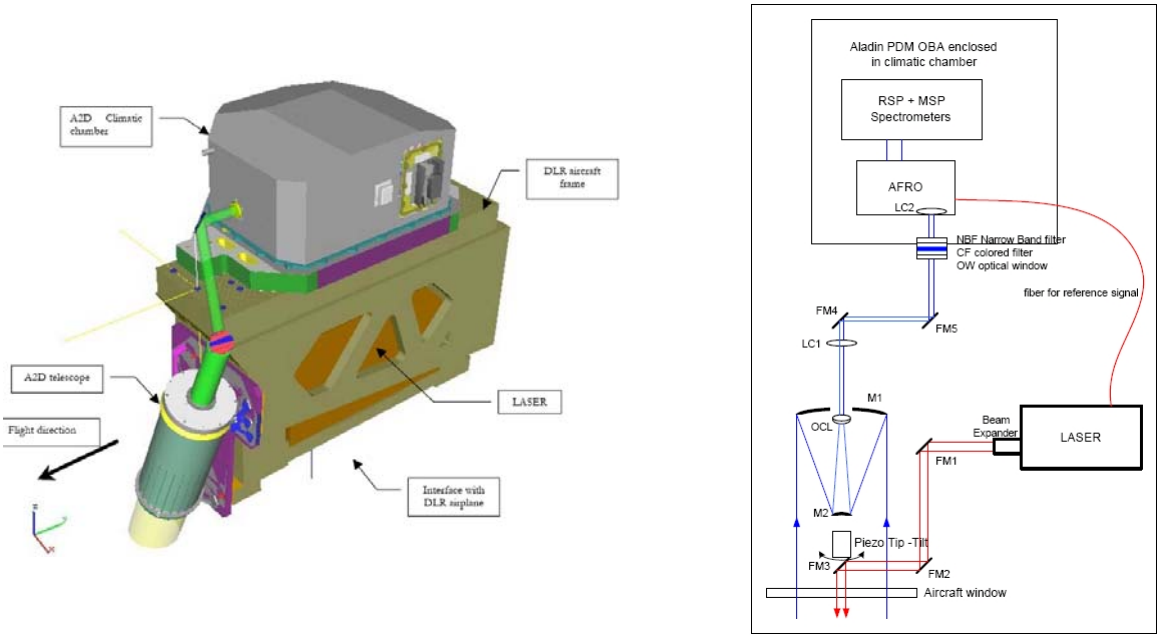

Figure 7: mechanical configuration of the main units of the A2D assembled on the airborne frame (left) and functional description of the A2D (right)

3.1 The A2D units characterisation

3.1.1 Airborne Front Optics (AFRO)

The front optics of the PDM receiver optical bench assembly (OBA) has been replaced to adapt it to the specific A2D needs. The AFRO functions are manifold. It includes a UV CCD camera registered on the field stop to locate the received spot and drive the co-alignment control loop to correct for the emission-reception misalignment. The AFRO is used as well to adapt the received signal to the ACCD dynamic range. Due to the backscattering of the atmosphere immediately below the airplane, a fast electro-optics modulator had to be introduced in the receiver path to attenuate the first microseconds of the return signal. The modulation occurs during a 70 µs period after each pulse. In order to avoid the ACCD saturation, the adjustment dynamic shall be 15 to 1. It was measured higher than 60 to 1. The AFRO includes the optical path to couple a fraction of each laser pulse to the receiver for calibration purposes. A field stop limits the receiver field of view to 1 mrad at the intermediate focus of a beam expander. The beam expander is used to expand the beam up to 20 mm, which corresponds to the nominal spectrometer input. At last the AFRO converts the incoming circularly polarised light to a linear polarisation perpendicular to the OBA baseplate, as needed by the spectrometer. A picture of the AFRO with all its optical component except the calibration fiber is shown in Figure 8.

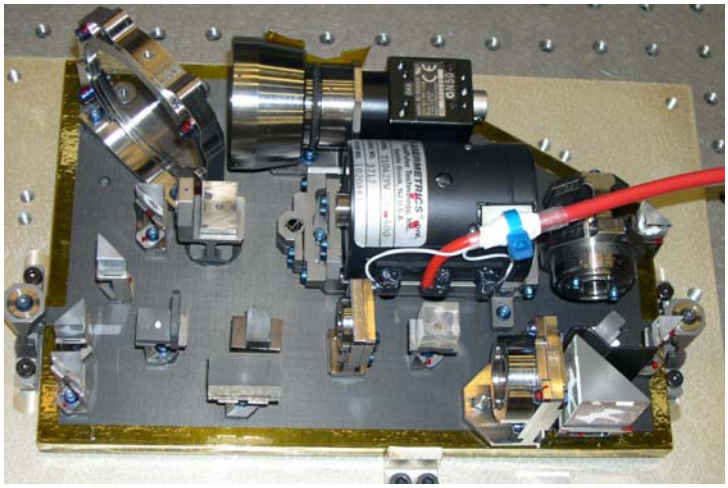

Figure 8: AFRO on its isostatic mounts

The AFRO has been fully characterized and has been submitted to temperature cycles from +5 ºC to +45 ºC to fix the micro-settlings and check the thermo-mechanical stability. The WFE was measured by use of a HASO wave front analyzer. This was done at 355 nm, before and after thermal cycling and the WFE amounts to 70 nm rms. The divergence (hence focus) was estimated, before and after thermal cycling, by projection of the output beam on a screen, to be less than 0.5mm at 5.4 m, i.e. less than 90µrd. Only the transmission is lower than expected (41%), likely due to non-conformances of the coating applied on some optics.

3.1.2 Telescope

The telescope has a 200 mm input diameter limited by the volume constraint within the Falcon20 aircraft. It is tilted only 20 º also because of volume constraint. This slant angle modification with respect to the satellite baseline (35 º) has some impact on the receiver sensitivity without impairing the performances in the airborne configuration. The telescope's mirrors have been taken from a commercial astronomy Perl-Vixen VC200L Cassegrain telescope (d=200mm, f/d=9). It has a sixth-order aspheric primary mirror (f=700mm), a convex spherical secondary mirror (75mm diameter) and a 3-lens field corrector. The telescope and each of its elements has been measured and characterized (WFE, transmission). The mirrors have been re-coated with a dielectric UV coating including the aspheric primary mirror. In order to check the re-coating process the mirrors underwent 10 thermal cycles from +5°C to +45°C as ageing test and showed no signs of pealing or cracking and no change in WFE. The reflection at 355 nm has been enhanced from 75 % to 99%, allowing to compensate for the low AFRO transmission.

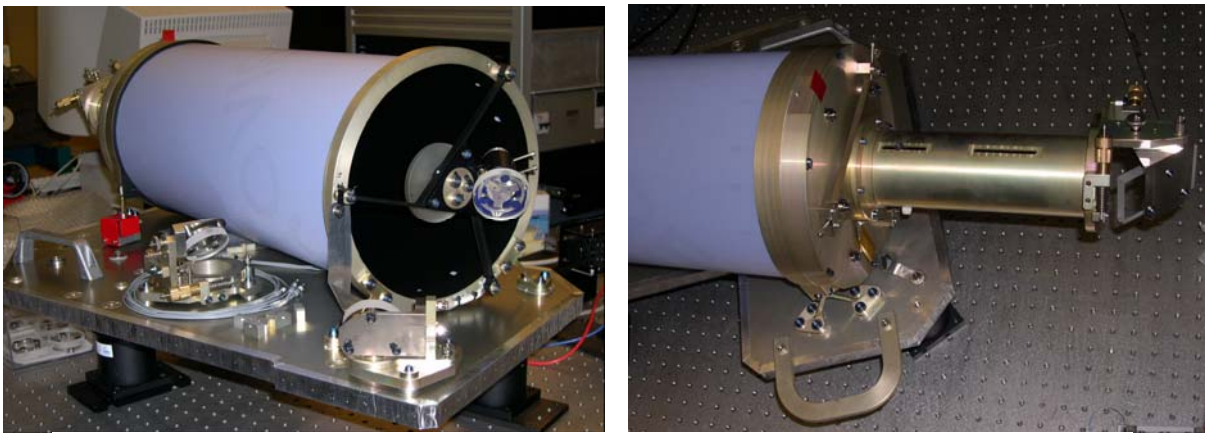

Figure 9: View of the telescope from the input side (left) including the piezo-mounted mirror and from the output side (righ) including the eyepiece and the first folding mirror

The telescope magnification has been measured to about 21 and its overall transmittance at 355 nm amounts to 76.1 % including the eyepiece lens and the obscuration. Its WFE including the ocular remains below 108 nm rms, well within specifications. For the rigidity of the design, an invar tube (0.5 mm thick) has been used and the first eigenfrequency lays 20 Hz above the required 60 Hz. From mechanical analyses, the telescope is compliant to the load requirements (crash loads amount to 9 g in flight direction) and the stability (defocus and rotation of the two mirrors) is calculated within the temperature ranges. Two views of the telescope including routing optics is provided in Figure 9.

3.1.3 Routing optics

The telescope is coupled to the OBA by free space propagation of a collimated beam, with pupil conjugation, which relaxes the constraints on their relative alignment. This coupling is achieved by a dioptric bloc, made of commercially available lenses, which have been defined and optimized using CODE V software. This bloc is also optimized to reduce any residual spherical aberrations, somewhat replacing the original field corrector.

Furthermore 3 folding mirrors are used to guide the emission beam from the output of the laser source to the atmosphere. The last emission mirror is mounted on a piezo tip/tilt actuator on the backside of the secondary mirror of the telescope. It is used to dynamically control the co-alignment of the emission beam and the receiver optical path.

At the reception, two folding mirrors are used to couple the output beam of the telescope to the input of the AFRO. Large folding angles are necessary, resulting in large mirrors. The incidence angles being fairly far from 45 º, custom coating have been deposited.

3.1.4 Climatic chamber

The whole OBA is covered by a temperature controlled climatic chamber (OBA climatic chamber: OCC) as shown in Figure10. It aims at maintaining the spectrometer within a very stable temperature in spite of the temperature range inside the aircraft during operation. Besides it ensures protection of the optics in the dusty environment of an airplane. The OCC is designed to maintain the OBA temperature between 15 ºC and 25 ºC with gradients in plane direction below 2 ºC, gradients in transverse direction below 0.5 ºC and a stability of 1 ºC between on ground operation and the end of measures flight. The equipments operating temperatures have to be maintained within 1 ºC and for the Rayleigh spectrometer, within 50 mK. The OCC provides a radiative and free convective control of the OBA and the internal side temperature is controlled by 4 thermo electric coolers cooled by water exchangers. To limit heat leaks from ambient to OBA enclosure, an insulating Melamine Basotect foam is fixed on the cover.

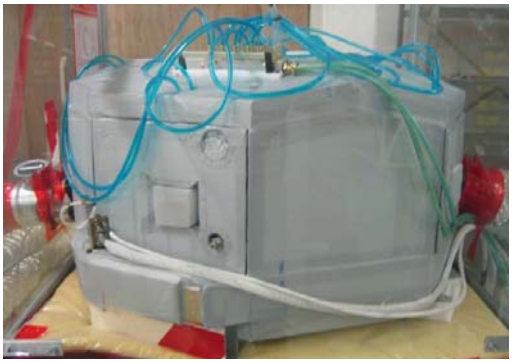

Figure 10: OCC in thermal test configuration; the melamine Basotect foam is covered by Terul sheets and assembled by pins on OCC.

The OCC was tested trough a thermal test campaign. The Rayleigh temperature stability was reached within one hour and held at 22.8 ºC with 30 mK pkpk variation even with environment at 35 ºC. The behaviour of the system was tested with respect to an interruption of the power, which is imposed during roll-out, fuelling and check-up phases of the aircraft during campaign operation. The RSP temperature is still in the stability range after one hour without power in the system. The results of the thermal tests are displayed in Figure 11 where the temperature sensors provide evidences of the capacity of the OCC to shield the OBA from external temperature variations. The control laws coefficients have been optimised to provide robustness to external environmental changes, improving the convergence speed and the stability.

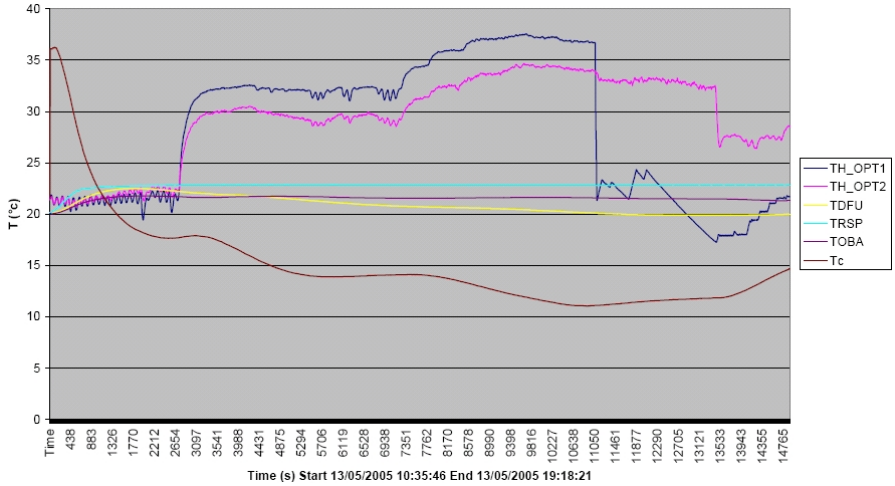

Figure 11: Overall behaviour of the thermal regulation system with the environment temperature going over 35 C (average of pink and dark blues lines until 11000s). The steep change in the dark blue line is caused by the thermistor position change into the cooler bath.

3.1.5 Ground support equipment

All the equipments necessary to run the ground and airborne campaigns have been manufactured and tested. Inside the aircraft, the frame on which the transmitter, the receiver and the telescope will be mounted has been refurbished from an existing frame. The transmission of the aircraft windows with a diameter of 515 mm has been measured in 77 positions in the UV to a mean transmission of 90.3% and a standard deviation of 1.3 %.

In order to characterise the shot-to-shot spectral behaviour of the laser a heterodyne unit assembly has been manufactured and successfully tested. It will be integrated in a 19" drawer module for use during flights.

The ground container where the integration and the ground campaigns will take place is fully operational. It is equipped with air-condition and radiator for thermal control. A ground support structure has been developed to lift the A2D into its final vertical position and to carry the bottom mirror needed in the ground configuration to steer the beam upward to the atmosphere. A second mirror on the roof of the container allows a pointing between 70º and 90 º; without the second mirror, the pointing is adjusted by the bottom mirror around the zenith direction at ±10º as depicted in Figure 12. Both mirrors are synthetic fused silica with HfO2/SiO2 HR coatings at 355 nm, optimised for each nominal working angle.

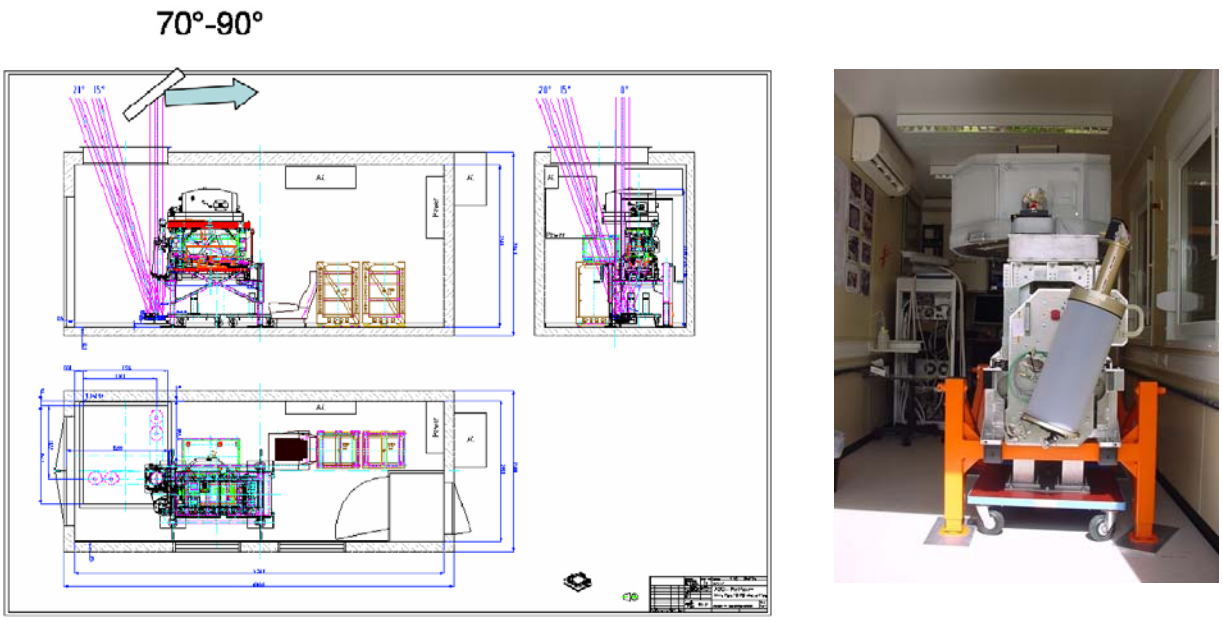

Figure 12: The different configurations of the A2D inside the ground container (left). Ground support structure with the A2D frame on top of it inside the ground container equipped with the telescope and the OCC(right)

4. CAMPAIGNS OBJECTIVES

The instrument concept of ALADIN combines new techniques, like a novel combination of the molecular and aerosol receiver, and the use of an Accumulation Charge Coupled Device ACCD to improve detection sensitivity. Also the use of a sequential Fabry-Perot with different maximum transmissions and spectral widths for the two channels of the Fabry-Perot was never applied before. There is a need to validate these features from ground and from aircraft, which is the most comparable to the downward looking geometry from space. Also the use of novel technologies within this instrument raises several topics for the ground processing algorithm development, which can be optimized with datasets from real atmospheric measurements.

Several ground campaigns have been performed in the past to validate the incoherent Doppler lidar principle through comparisons of radiosondes wind profiles with lidars based on double edge technique at 355 nm [6,7]. Comparisons of wind measurements from incoherent detection Doppler lidars with coherent Doppler lidars and other sensors were made in Europe [8,9] and USA [10]. Up to now no direct detection Doppler lidar was operated onboard an aircraft, whereas airborne validations of coherent Doppler lidars were performed in the last years [11,12]. A comparison of LOS wind profiles from a radar profiler with a coherent Doppler lidar has been published [13], which presents a similar approach as foreseen for the ADM-Aeolus ground campaign.

The main objectives of the ADM-Aeolus campaigns are the validation of the predicted instrument radiometric and wind measurement performance, and the establishment of a dataset of atmospheric measurements obtained with an ALADIN

type instrument to improve algorithm development for L1B (uncorrected horizontal line-of-sight HLOS wind speed), L2A (aerosol and cloud products) and L2B products (corrected HLOS wind speed).

Due to the airborne constraints imposed by the geometry (Figure 13), the following differences of the ALADIN Airborne Demonstrator A2D and the satellite ALADIN instrument will be taken into account in the analysis of the data, the adaptation of the processing algorithms and the conclusions:

- Same timing of ACCD with minimum readout of 2.1 µs (315 m) results in different vertical ranges (296 m at 20° nadir instead of 251 m at 37° nadir)
- Different horizontal resolution for 700 shots: 2.8 km instead of 50 km
- Co-axial transmitter/receiver telescope arrangement instead of transceiver-telescope
- Receiver FOV 100 µrad instead of 20 µrad => footprint on ground Ø 1 m from range 11 km instead of Ø 10 m from 500 km
- Difference in front-optics (Airborne Front Optics AFRO) with Electro-Optical Modulator EOM and additional CCD for co-alignment of laser transmitter and telescope FOV
- Quasi-continuous operation (4 s readout for 14 s measurement) instead of burst mode operation with laser PRF 50 Hz instead of 100 Hz
- Known imperfections in the Pre-Development Model spectrometers (ghost images, polarising beamsplitter problems, transmission losses, spacing Rayleigh Fabry-Perot 2.65 pm instead of 2.3 pm) instead of "perfect" Flight Model
- Reference pulse from transmitter is accumulated with the same number of shots than atmospheric signal instead of single shot acquisition => but single shot acquisition will be realised with separate heterodyne unit
- energy*aperture/range2 product (70 mJ, Ø 0.2 m, 11 km) is 17 times higher than satellite (150 mJ, 1.5 m, 500 km)
- Different sensing ranges of 11 km (10 km, 20 °) instead of 500 km (408 km, 35 °) lead to different dynamical range of signal => strong signal dynamics for airborne platform instead of "flat" dynamics from satellite due to 1/R2-factor

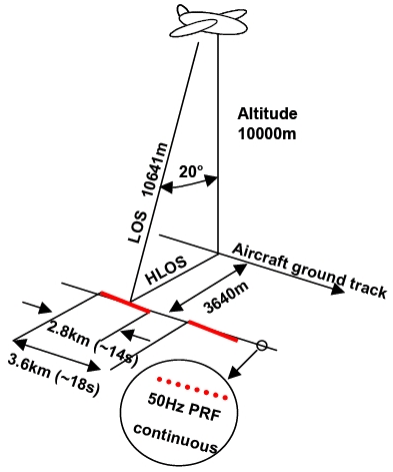

Figure 13: Aeolus airborne campaign geometry

The baseline for the Aeolus Ground Campaign (AGC) is a 4-week campaign in April 2006 at the Meteorological Observatory Lindenberg MOL of the German Weather Service DWD close to Berlin. The main reference instruments for comparison will be a 2 µm Doppler lidar from DLR [14,15], and a 482 MHz windprofiler radar WPR from DWD. Additional instruments from DWD-MOL will be operated to allow comprehensive characterisation of the A2D under various atmospheric conditions: a laser ceilometer, a sun-photometer, additional radiosondes Vaisala RS92- SGP, and a cloud-radar. For evaluation of the received backscatter intensity of the A2D, an aerosol lidar operating at 355 nm from the Meteorological Institute of the University Munich MIM will be deployed [16].

The objectives of the AGC, are by order of priority, the radiometric performances, the spectrometers response calibration, the wind velocity performance, the assessment of the A2D LOS measurement statistical error, the development of Quality Control and correction scheme for homogeneous and inhomogeneous conditions (clouds, aerosols, wind shear), aerosol products. Other implicit objectives of the AGC are preparation of the airborne campaigns, optimisation of alignment, calibration and measurement operations and characterisation of A2D functionality over an intensive measurement period.

The first airborne campaign (AC01) follows a 4-week ground based campaign AGC and two technical flights during which the lidar will be characterized at ground and functionally tested in flight. The AC01 campaign is thus an intermediate step. The main objective is to verify that the airborne implementation of the A2D is correct and the system is ready for the extensive campaign AC02. Besides, data acquired during this campaign will be delivered to the teams working on the Aeolus data processing and used to check the algorithms are working properly.

AC02 will be, towards the beginning of 2007, the second and longer airborne campaign during which extensive measurements will be acquired with the objective to test the processing chain of ADM-Aeolus and the ability of the space-borne system to make useful observations in a real atmosphere, including its anticipated heterogeneities. As a consequence, the power and spectral characteristics of the signal are verified, procedures to determine aircraft-induced Doppler shift, line-of-sight direction and ground surface velocity are validated, and the quality of data is checked against a “ground-truth” for homogeneous, but also for some atmospheric heterogeneous cases.

5. CONCLUSIONS

Measurements of wind fields are essential for Numerical Weather Prediction and Climate studies. A spaceborne Doppler Wind Lidar (DWL) is the only candidate instrument to provide global and direct three-dimensional wind measurements.

The Aeolus mission concept has been proposed based on an innovative incoherent lidar principle, though using mature space technologies. The concept is based on an incoherent UV receiver with a tripled-frequency Nd:YAG laser. It fulfils the specifications of a demonstration mission and will provide wind measurements on a global scale with a similar accuracy than conventional rawindsonde observations.

The ALADIN airborne demonstrator is under development aiming at a first ground campaign in spring 2006 at the site of the Meteorological Observatory Lindenberg, Germany. The first aircraft campaign will follow in autumn 2006 providing the first real atmospheric data from a direct detection Doppler lidar ever. The A2D and a coherent 2 μm Doppler lidar will be used simultaneously providing a unique setup where incoherent and coherent detection lidar can operate on the same atmospheric volume. The downward looking instrument will provide realistic data which cannot be obtained from the ground instruments, where effects such as cloud spatial variability, ground return signal at the end of the backscatter signal are absent. Moreover, from a high flying aircraft, the signal dynamics of the aerosol and molecular channels are closer to that expected from space. Such data will be valuable for the finalisation and validation of the ground processing algorithms and for deriving quality control schemes and to assess errors of calibration schemes and temperature/pressure corrections. Besides, the campaigns will enable to validate the calibration procedures of the instrument This will be a key step in the path to the first lidar mission to sense the global wind field from space.

REFERENCES

1. *Statement of guidance regarding how well satellite capabilities meet WMO user requirements in several applications area*, Sat-26, WMO/TD No. 1052, 2001

2. *Atmospheric Dynamics Mission, Report for Mission*, ESA-SP-1233(4), 1999

3. M. Endeman, P. Dubock, P. Ingmann, R. Wimmer, D. Morançais, D. Demuth, *The ADM-AEOLUS mission – The first wind-lidar in space*, Proc. 22nd International Laser Radar Conference (ILRC 2004), ESA SP-561, p 61-64, June 2004

4. M. Schillinger, D. Morançais, F. Fabre, A. Culoma, *ALADIN: the LIDAR instrument for the Aeolus mission*, Proc. SPIE Int. Soc. Opt. Eng., **4881**, 40-51 (2002)

5. Y. Durand, R. Meynart, A. Culoma, D. Morancais, F. Fabre, *Results of the pre-development of ALADIN, the direct detection Doppler wind lidar for ADM-Aeolus*, Proc. SPIE Int. Soc. Opt. Eng. **5570**, 93-104 (2004)

6. C. Flesia, C. L. Korb, Ch. Hirt, *Double-edge molecular measurement of lidar wind profiles at 355 nm*, Opt. Lett., **25**, 1466-1468 (2000)

7. B. Gentry, M., H. Chen, S. X. Li, *Wind measurements with 355-nm molecular Doppler lidar*, Opt. Lett., **25**, 1231-1233 (2000)

8. A. Delaval, C. Loth, P. H. Flamant, D. Bruneau, *Experimental Tests to Validate a Multiwavelength backscatter database*, Final Report VALID 1, CNRS/IPSL September 2000, 56 pages + annex.

9. A. Delaval, P. H. Flamant, C. Loth, A. Garnier, C. Vialle, D. Bruneau, R. Wilson, D. Rees, *Performance Validation of Direct Detection and Heterodyne Detection Doppler WIND Lidars*. Final Report VALID 2, CNRS/IPSL September 2000, 76 pages

10. R. M. Hardesty, W. A. Brewer, C. A. Nardell, B. W. Gentry, J. G. Yoe, J. M. Rya, *Intercomparison of Heterodyne and Direct Detection Doppler Lidars during the 2000 Bartlett, N. H., Measurement Campaign*, Proc. 11th Coherent Laser Radar Conference, Malvern, UK, 115-118 (2001)

11. O. Reitebuch, Ch.Werner, I. Leike, P. Delville, P. H. Flamant, A. Cress, D. Engelbart, *Experimental Validation of Wind Profiling Performed by the Airborne 10µm-Heterodyne Doppler Lidar WIND*, J. Atmos. Ocean. Tech. **18**, 1331-1344 (2001)

12. O. Reitebuch, H. Volkert, Ch. Werner, A. Dabas, P. Delville, Ph. Drobinski, P. H. Flamant, E. Richard, *Determination of air flow across the Alpine ridge by a combination of airborne Doppler lidar, routine radio-sounding and numerical simulation*. Q. J. R. Meteorol. Soc. **129**, 715-728 (2003)

13. S. A. Cohn, R. K. Goodrich, *Radar Wind Profiler Radial Velocity: A Comparison with Doppler Lidar*, J. Atmos. Ocean. Tech. **41**, 1277-1282 (2002)

14. S. Rahm, R. Simmet, M. Wirth, *Airborne two micron coherent lidar wind profiles*. Proc. 12th Coherent Laser Radar Conference, Bar Harbor, Maine, USA, 94-97 (2003)

15. F. Köpp, S. Rahm, I. Smalikho, *Characterisation of Aircraft Wake Vortices by 2µm Pulsed Doppler lidar*, J. Atmos. Ocean. Techn. 21, 194-206 (2004)

16. C. Böckmann, U. Wandinger, A. Alnsmann, J. Bösenberg, V. Amiridis, A. Boselli, A. Delaval, F. de Tomasi, M. Frioud, I.V. Grigorov, A. Hagard, M. Horvat, M. Iarlori, L. Komguem, S. Kreipl, G. Larcheveque, V. Matthias, A. Papayannis, G. Pappalardo, F. Rocadenbosch, J.A. Rodrigues, J. Schneider, V. Shcherbakov, and M. Wiegner, *Aerosol lidar intercomparison in the framework of the EARLINET project: 2. Aerosol backscatter algorithms*, Appl. Opt. **43**, 977-989 (2004)